A Micro Pattern Gas Detector for X-ray polarimetry

R. Bellazzini[a], F. Angelini[a], L. Baldini[a], A. Brez[a], E. Costa[b], G. di Persio[b], L. Latronico[a],M. M. Massai[a], N. Omodei[a], L. Pacciani[b], P. Soffitta[b], G. Spandre[a]

[a]Istituto Nazionale di Fisica Nucleare - sezione di Pisa,
via Livornese 1291, I-56010 San Piero a Grado (PI), Italy
[b]Istituto di Astrofisica Spaziale del CNR,
via Fosso del Cavaliere 100, I-00133 Roma, Italy

ABSTRACT

We report on a new instrument that brings high efficiency to X-ray polarimetry, which is the last unexplored field of X-ray astronomy. It derives the polarization information from the tracks of the photoelectrons imaged by a finely subdivided gas pixel detector. The device can also do simultaneously good imaging (50-100 μm), moderate spectroscopy (16% FWHM at 5.4 keV) and fast, high rate timing down to 150 eV. Moreover, being truly 2D, it is non dispersive and does no require rotation. The great improvement of sensitivity (at least two orders of magnitude) will allow direct exploration of the most dramatic objects of the X-ray sky; with integrations of the order of one day we could perform polarimetry of Active Galactic Nuclei at the per cent level, a breakthrough in this fascinating window of high energy astrophysics.

Keywords: X-ray Polarimetry, Photoelectric Effect, Gas Imaging Detectors

1. INTRODUCTION

1.1. The case for astronomical X-ray polarimetry

X-ray astronomy has lived, through the last 40 years, a long period of exciting discoveries and partially fruitful attempts to fit in a fully consistent theoretical framework such various objects like Super Nova Remnants (SNRs), Active Galactic Nuclei (AGNs), pulsars and black hole candidates. Despite this, physics is far away from being completely understood and many fundamental questions remain basically unanswered.

Most times theoretical models are compared with data only in relation with light curves and energy spectra; this happens because, due to the lack of efficient instrumentation, these are the only experimentally accessible informations[1]. The detection of linear polarization by Crab Nebula[2] (that dates from 1975) is, to date, the the only significant experimental result of astronomical X-ray polarimetry. In the Crab case synchrotron radiation from ultra-relativistic particles is now universally accepted as the dominant emission process; the verification of this hypothesis for others Super Nova Remnants would constitute a particularly interesting result, possibly helping to throw light over the origin and acceleration of cosmic rays, which is one of the most important unanswered question of high-energy astrophysics. In addiction to this, efficient polarimetry would be irreplaceable for the study of compact objects, since it often provides the *only* way to investigate the geometric structure of those sources (AGNs[3], isolated neutron stars[4], binary X-ray pulsars[5]) which cannot be directly *resolved.* Moreover, it is commonly believed that energy-resolved X-ray polarimetry would constitute one of the most direct probes of strong gravity effects in celestial sources, providing a straightforward signature of the presence of a black hole[6].

Further author information: (Send correspondence to Ronaldo Bellazzini)
Ronaldo Bellazzini: E-mail: ronaldo.bellazzini@pi.infn.it, Telephone: +39 050 880286, Address: via Livornese 1291, I-56010 San Piero a Grado (PI), Italy

Polarimetry in Astronomy, Silvano Fineschi, Editor, Proceedings of SPIE
Vol. 4843 (2003) © 2003 SPIE · 0277-786X/03/$15.00

1.2. Basic formalism

A traditional polarimeter typically consists of an analyzer and a detector, both rotating around their axis; in general a modulation of the counts (in the case of polarized radiation), at twice the rotation frequency, is observed:

$$N(\phi) = C_1 + C_2 cos^2(\phi - \phi_0). \tag{1}$$

The visibility of the modulation for 100% linearly polarized incident radiation

$$\mu = \frac{N_{max} - N_{min}}{N_{max} + N_{min}} = \frac{C_2}{2C_1 + C_2}, \tag{2}$$

is called *modulation factor* and constitutes the fundamental factor of merit for the instrument, spanning from 0 (insensitive device) to 1 (perfect polarimeter). The other important parameter is the so called *Minimum Detectable Polarization*, defined as the minimum modulated flux necessary to exceed, at a certain confidence level, fluctuations of both background and unmodulated signal. Assuming Poisson statistics in counting rate, it is possible to show that the MDP at the level of n_σ standard deviations can be written as

$$MDP(n_\sigma) = \frac{n_\sigma}{\varepsilon \mu F} \sqrt{\frac{2(B + \varepsilon F)}{ST}}, \tag{3}$$

where F is the source flux, ε the detection efficiency, B the background rate per unit of surface, S the collecting area and T the observing time. Since μ, ε, F and B depend on energy of incoming radiation (as well as S, in case the polarimeter is placed at the focus of a X-ray optics), expression 3 must be integrated over the whole energy range of interest. In any case, given the source and the characteristics of the detector, equation 3 allows to evaluate the integration time necessary to perform a planned measurement. We notice that, while for *bright sources* ($B << \varepsilon F$) the dependence of MDP from modulation factor and detection efficiency can be written as:

$$MDP \propto \frac{1}{\mu \sqrt{\varepsilon}}, \tag{4}$$

in the limit $B >> \varepsilon F$ (*faint sources*) MDP scales as:

$$MDP \propto \frac{1}{\mu \varepsilon}. \tag{5}$$

That is, polarimeter's efficiency play a different role in different physical situations; in the case of strong sources, which is quite common at the focus of a X-ray optics, modulation factor is the leading merit factor and the dependence of MDP on detection efficiency is weaker.

1.3. Traditional techniques of X-ray polarimetry

Bragg diffraction at 45° and Thomson scattering at 90°, exploited in Ariel 5 and OSO-8 mission, remain, to date, the standard techniques of astronomical X-ray polarimetry; nevertheless, it is rather hard to imagine substantial developments within this framework.

A flat planar crystal, oriented at 45° with respect to an incident beam of X-rays, is a perfect polarization analyzer for photons satisfying Bragg law; only the radiation which is polarized perpendicularly to the incidence plane is reflected and, by rotating the crystal around its axis, a linear polarization of the beam results in a modulation of counts at twice the rotation frequency (Fig. 1). Despite the high modulation factor generally obtainable within this technique, Bragg polarimeters are typically very narrow-band instruments (graphite, for instance, even though it is a high integrated reflectivity crystal, provides a bandwidth of only 4 eV at 2.62 eV) and moreover they are dispersive and not tunable in energy.

The dependence of Thomson cross section from the direction of polarization of the incoming photon can be alternatively exploited to build a polarimeter (Fig. 1); the radiation scattered at 90° with respect to the incident beam has a distribution:

$$I(\phi) \propto sin^2\phi, \tag{6}$$

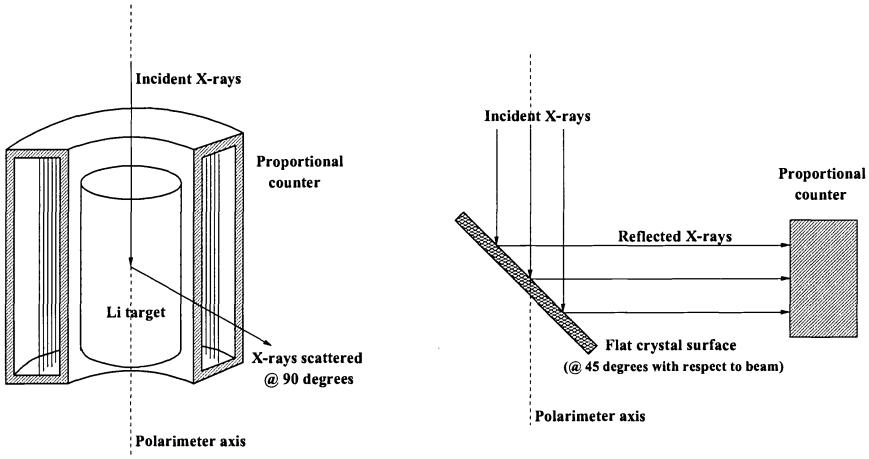

Figure 1. Typical examples of Thomson (left) and Bragg (right) polarimeters. In the first case a proportional counter surrounding the lithium target detects the X-rays scattered at an angle close to 90°, while the Bragg polarimeter consists of a planar crystal oriented at 45° with respect to the incident beam and a counter detecting reflected radiation.

and so the angular distribution of the diffused X-ray is modulated by the polarization of incoming radiation. The main limit, in this case, is that in the few keV range (where the sources are brighter and the optics are very efficient) Thomson scattering is a vastly depressed process, if compared with photoelectric absorption; even in a low-Z element like lithium photoabsorption cross section is three orders of magnitude greater than scattering cross section at 1 keV and still one order of magnitude greater at 5 keV. Moreover, Thomson formula is 100% modulated only for 90° scattering angle, which strongly limits the modulation factor one can reach.

It is clear that possible further improvements within traditional techniques described above are intrinsically prevented from severe physical (more than technological) limitation. It is also worth to note that they require double-stage devices that need to be rotated, giving rise to the additional difficulty to control systematic effects at the few percent level, as requested for the most interesting measurements.

2. THE MPGD AS A POLARIMETER

2.1. Photoelectric effect

At low energy photoelectric absorption is the physical process with the greatest cross section. In the case of linearly polarized X-rays the angular distribution of the emitted electrons, when projected on the plane perpendicular to the incident radiation, has the characteristic electromagnetic $cos^2 - like$ shape (it basically derives from the scalar product $\mathbf{p} \cdot \mathbf{A}$ between the electron momentum and the photon electric field constituting the interaction Hamiltonian) somewhat convoluted with the initial wave-function of the bound electron. In the case of a s-orbital (which is spherically symmetric) it is then quite natural to expect a pure $cos^2 - like$ angular distribution.

Actually, working out the calculation[7], one finds that the non relativistic, polarized photoemission cross section, in this case, is given by:

$$\frac{d\sigma}{d\Omega} = r_0^2 Z^5 \alpha^4 (\frac{m_e c^2}{h\nu})^{\frac{7}{2}} \frac{4\sqrt{2} sin^2\theta cos^2\phi}{(1-\beta cos\theta)^4}, \tag{7}$$

where θ is the polar angle between the direction of propagation $\mathbf{k}$ of the incoming photon and the direction of emission, ϕ the azimuthal angle measured starting from the direction of polarization of the radiation and β is the final velocity of the photoelectron in terms of the speed of light. So the photoelectron is emitted preferentially in

the plane orthogonal to **k** (due to the sin^2 term) and along the electric field of incoming photon. As expected, the projection of the expression 7 on the plane orthogonal to **k** is

$$\frac{d\sigma}{d\phi} \propto cos^2\phi, \tag{8}$$

that is, it is completely modulated by the polarization of the incoming radiation.

Photoemission cross sections can be derived for p, d and f orbitals; as we aspect, they are less modulated due to aspherical shapes of initial electronic wave functions. The point here is that, when the photon energy is greater than K-edge of absorbing material, K-shell electrons constitute the dominant contribute to total cross section, so that expression 7 provide an accurate description of the whole process.

2.2. The Detector

Polarimetric capabilities of photoelectric effect have been recognized since long time ago. The problem is that, at the energies of interest, electrons propagate in matter less than photons; for instance the range of a 5 keV electron, even in a light gas like neon, is no more than some hundreds of μm (just for comparison, it is less than 1 μm in silicon). Nevertheless the reconstruction of such a short track is now possible with a finely segmented gas detector.

Figure 2 shows a schematic view of a Micro Pattern Gas Detector suitable for X-ray polarization measurements[8]. Incoming photon, entering orthogonally to the detector through a thin mylar window, is absorbed somewhere in the upper, gas-filled gap. The photoelectron, preferentially emitted onto the detector plane (according to equation 7), interacts with the gas leaving along its track a certain number of ion-electron pairs; in order to

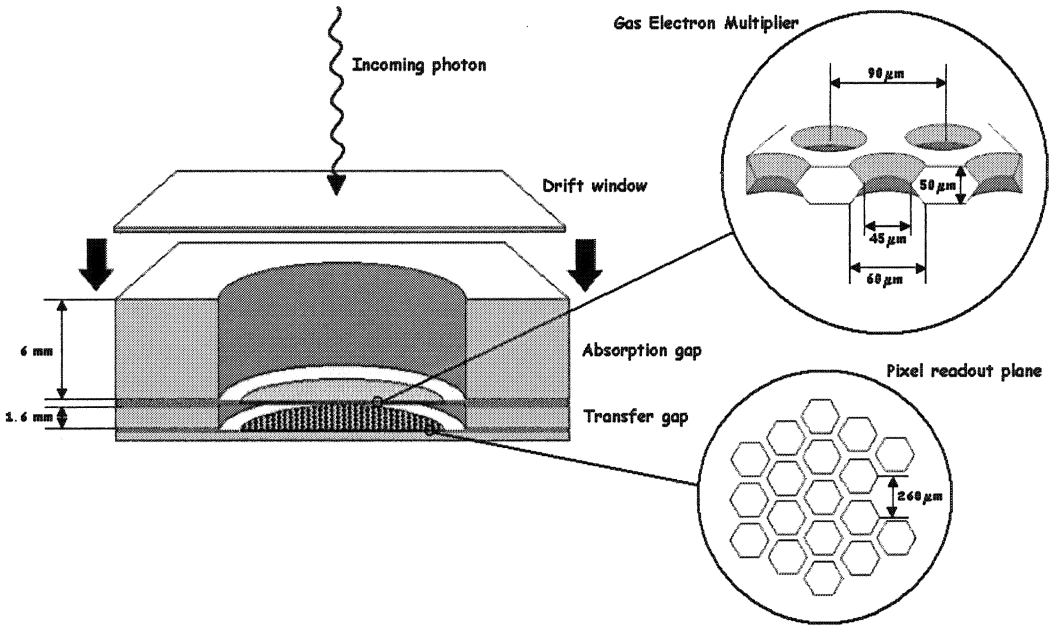

Figure 2. Schematic cross section of a MPGD for polarimetric application; dimensions quoted are those of the prototype under test in our laboratory. Gas Electron Multiplier consists of a thin kapton foil, metallized on both sides and etched with a regular matrix of holes; the application of a suitable difference of potential between the electrodes create an intense electric field providing very granular gas multiplication and high efficiency in charge transfer. Pixel readout is organized in a hexagonal pattern in order to improve track reconstruction accuracy, minimizing angular non-linearity due to the sampling.

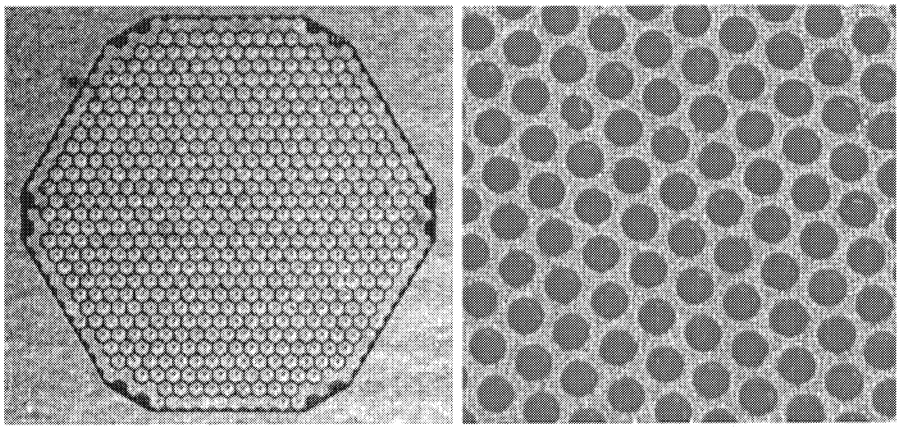

Figure 3. Photomicrographs of the MPGD prototype under test: the readout plane (left) and the gas electron multiplier (right).

collect this charge, a drift electric field is established by applying a difference of potential between the electrodes. Electrons are transported toward the Gas Electron Multiplier[9], which provides the necessary gas gain, and finally collected on pixel readout plane (figure 3), allowing track reconstruction.

It is worth it to note that only electrons moving from the bottom side of the GEM toward the anode pixels after *avalanche* multiplication contribute to the signal. If we suppose the electric field constant within the transfer gap (which, far from the GEM, is quite a reasonable approximation), the charge inducted on the readout plane from an electron placed at a distance x from the bottom side of GEM is:

$$Q = +e\frac{x}{d}, \tag{9}$$

where d is the total thickness of transfer gap. The current inducted on the anode can be expressed, in terms of the drift velocity v of the electron, as:

$$I = -\frac{dQ}{dt} = -e\frac{v}{d}, \tag{10}$$

and the duration of the signal is then of the order of d/v (which is about 30 ns for v $\simeq$ 5 cm/μs and d $\simeq$ 1.5 mm). This means that, with a suitable front-end electronics, our detector is naturally capable of high-rate precise timing. We also note that, since the total released charge is proportional to the energy of the incoming photon, the instrument can perform spectroscopy at the level of a good proportional gas detector; moreover, thanks to the 2-D micro-structure of readout electrode, it is naturally imaging and does not need to be rotated.

The MPGD described here basically combines the best performance of gas detectors: high granularity, fast signal and reasonable energy resolution; it's a kind of modern, compact, self triggering cloud chamber providing spectral capabilities.

2.3. The role of gas mixture

Photoelectron releases its energy in the gas mainly through inelastic collisions with atomic electrons, while Coulomb interaction with nuclei deflects it from the original direction; we stress the fact that, for our purposes, electromagnetic scattering is a particularly undesirable process to occur: being substantially elastic, it leaves no trace within the detector and, at the same time, it causes a progressive randomization of photoelectron track (which is what we want to reconstruct).

Photoelectron energy loss is described by the Bethe-Bloch formula; it is basically proportional to atomic number of absorbing material and to the inverse of electron kinetic energy:

$$\frac{dE}{dx} \propto \frac{Z}{E}. \tag{11}$$

On the other hand, elastic scattering on nuclei follows a screened Rutherford cross section, whose dependence on Z and E is given by:

$$\sigma_{Rutherford} \propto \frac{Z^2}{E^2}. \tag{12}$$

The point here is that, while slowing down is proportional to the atomic number of the gas, scattering cross section increases as Z^2; since we are interested in keeping the scattering / stopping-power ratio as small as possible, low Z mixture are in principle better for our applications, although obviously heavier gases provide higher detection efficiency.

Moreover, light mixtures typically have a low K-shell and that is a desirable feature for several reasons: first of all it allows to reach high modulations at low energy (because the direction of emission is less modulated for p, d and f orbitals); then the Auger electron, isotropically emitted as a consequence of atomic relaxation, bears only a little fraction of available energy and does not blur the photoelectron track. Finally, in a low Z gas, tracks are longer and then easier to reconstruct.

Diffusion of primary ionizazion during the drift toward GEM is another key-point; in principle thick absorption gaps provide greater detection efficiency, but diffusion has the effect of smearing the charge pattern, blurring in part the directional information; this effect can be limited by adding to the mixture complex molecules increasing the drift velocity and decreasing as a consequence the diffusion. In any case, once the gas mixture is chosen, this fixes the limit for the absorption gap thickness.

Leaded by all these considerations we have chosen for our tests a neon based gas mixture, with the addiction of a small amount of Dimetilether (DME) as a *quencher*; but we remark that the choice of the gas (and pressure) is a fundamental point that can only be completely worked out depending on the physical targets.

3. EXPERIMENTAL SETUP AND RESULTS

3.1. Experimental setup

A flow diagram representing the experimental setup is shown in figure 4. The signal induced by the avalanche on the top side of the GEM, amplified and discriminated, provides the trigger for the front-end electronics. We have used an hybrid originally studied for the CMS tracker, in the configuration optimized for Micro Strip Gas Chambers; it consists of four chips, for a total of 512 independent electronic channels each made of a preamplifier and a 45 ns peaking time shaper. The employed electronics is mainly designed to achieve a fast time response,

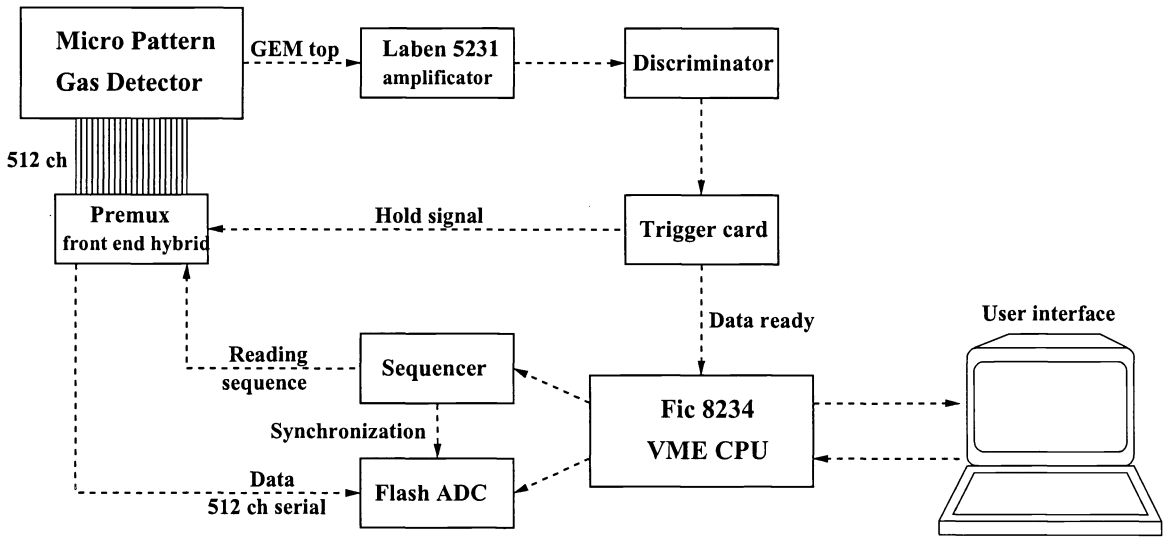

Figure 4. A schematic diagram of our Data AcQuisition system.

but it is worth to note that, with a limited counting rate (which is the typical situation in space application), a slower chain could provide better performance in terms of noise and energy resolution. Data acquisition system consists in two VME modules (a sequencer and a flash ADC) and a trigger card, all controlled by a VME CPU.

For the prototype under test, the readout plane is subdivided in hexagonal pixels with a pitch of $200\mu m$; the fan out to the front-end electronics has been realized with a multilayer technology on seven superimposed kapton foils. The technological effort, here, is to read out 512 independent electronic chains from a few mm^2 active area using essentially a Printed Circuit Board (PCB) technique. The GEM is a $50\mu m$ thick kapton foil metallized on both sides with $4\mu m$ copper while holes ($60\mu m$ in diameter) are organized into a $90\mu m$ pitch triangular matrix. The mechanics of the detector is quite simple, consisting in a $6mm$ thick fiber-glass spacer for the absorption gap and in a $1.6mm$ thick teflon one for the transfer gap;an aluminated mylar drift window is directly glued onto the top of absorption gap. A 1 Atm Ne/DME 80/20 gas mixture has been used throughout all measurement described in this paper.

We have tested the detector with both unpolarized and polarized radiation. Unpolarized photons come from a ^{55}Fe radioactive source emitting at $5.9keV$; a collimator, placed directly on drift plane, limits incidence angle to values close to 90° (±4°) with respect to the detection plane. Polarized radiation is obtained by scattering at 90° with a Li target photons produced by a X-ray tube; a double diaphragm collimator limits the scattering angles at 90° ± 5° so that the radiation entering the detector is linearly polarized for a fraction greater than 98%. In this case the spectrum is composed by a fluorescence peak of the anode ($5.4keV$ for Cr and $8.0keV$ for Cu) superimposed to some bremsstrahlung contaminations which have been reduced as much as possible during the analysis by pulse height selection.

3.2. Results

Details of analysis algorithms will be discussed in an accompanying paper[10]; basically, the direction of emission of the photoelectron is reconstructed by evaluating the major principal axis of the charge distribution collected by the pixel readout plane. Even if the range of a 5 keV electron in our gas mixture is few hundreds μm, we are able to *resolve* the track (figure 5). As already stated, the original direction of emission of the photoelectron, projected onto the plane of the detector, is completely modulated by photon polarization, but electromagnetic scattering introduces a partial randomization of the tracks; at the end, what we expect, in the case of 100 % polarized radiation, is a distribution modeled by the function

$$N(\phi) = C_1 + C_2 cos^2(\phi - \phi_0), \tag{13}$$

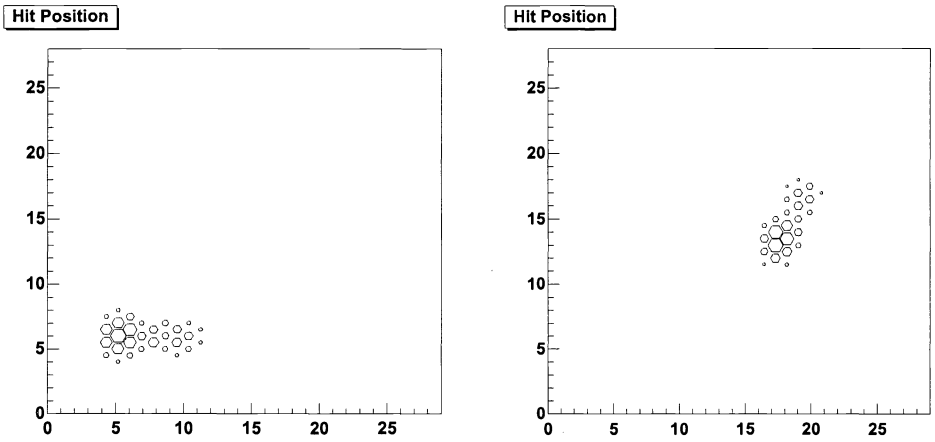

Figure 5. Sample tracks collected irradiating the detector with 5.9 keV unpolarized X-rays (the gas mixture is Ne/DME 80/20 at 1 Atm). The area of each exagon is proportional to the charge inducted to the corresponding pixel of the readout plane.

that takes into account both effects. In figure 6 experimental results are shown for both unpolarized and polarized radiation. In the first case, as we aspect, the angular distribution of the tracks is flat while in the latter it is peaked in correspondence of polarization angle of incoming radiation.

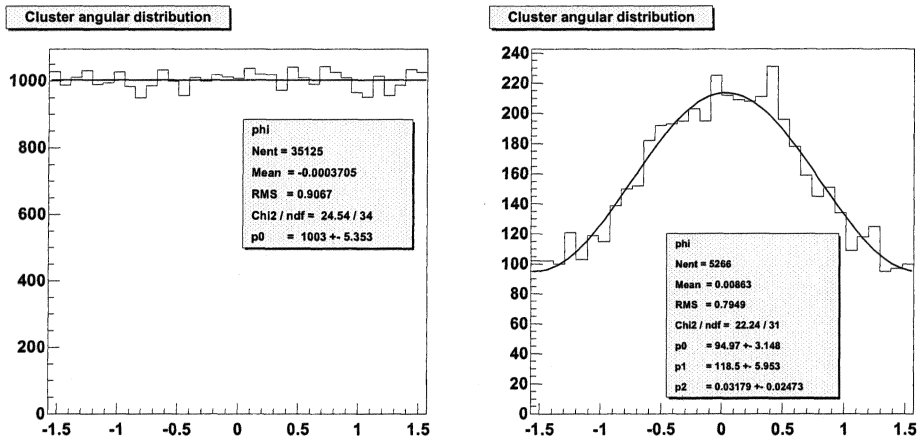

Figure 6. Polarimeter response to 5.9 keV unpolarized (left) and 5.4 keV polarized (right) radiation. Plots refer to two runs taken in identical experimental condition.

The direction of X-ray polarization with respect to detector can be freely changed by simply rotating the detector itself around beam axis; a fit to the data with the function (13) provides the best value ϕ_0 for the reconstructed polarization angle. In figure 7 the reconstructed angle is plotted against the *real* polarization angle, obtained by precisely measuring the orientation of the detector with respect to the output direction of the X-ray tube beam; the plot confirm the excellent angular linearity of the instrument and rules out the presence of systematic effects or non-linearity due to preferred directions in the readout sampling pattern.

As stated in Section 2, the MPGD is basically a proportional counter. In figure 8 the energy response (obtained by summing the signals induced on all fired pixels) to the ^{55}Fe line is showed; detector provides the

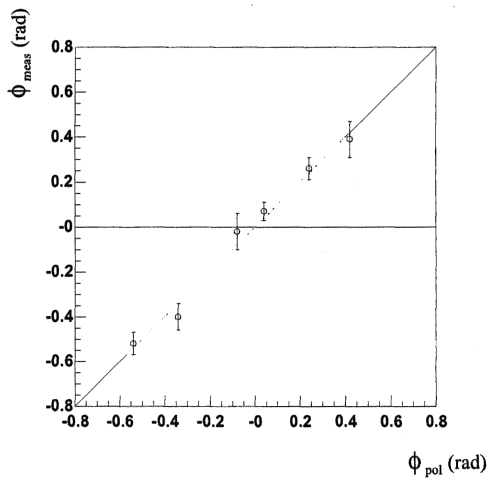

Figure 7. X-ray polarization angle as evaluated from a fit to data (ϕ_{meas}) plotted against the angle measured from the orientation of the detector with respect to the beam (the graph refers to 5.4 keV polarized radiation). The line represents the ideal line $\phi_{meas} = \phi_{pol}$.

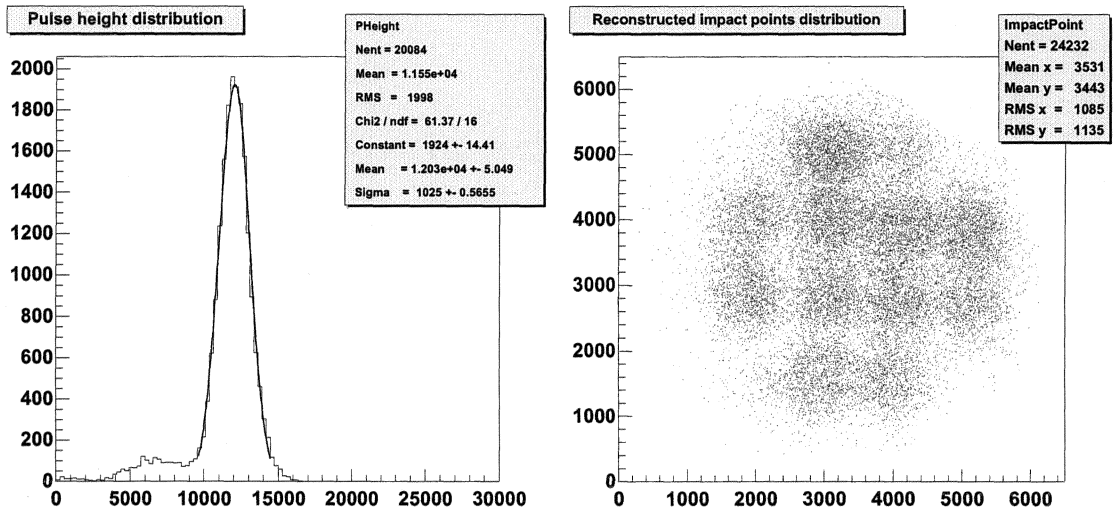

Figure 8. MPGD energy response (left) to the ^{55}Fe 5.9 keV line. The low energy tail is due to not fully contained events; the energy resolution is 20% FWHM. Imaging capabilities of the detector (right) when irradiated with 5.9 keV unpolarized radiation through a collimator with $500\mu m$ diameter holes and $1mm$ pitch. The distance between the peaks (fitted with gaussians within suitable subranges) are in excellent agreement with nominal values of the collimator.

typical energy resolution of a good gas detector, which is of the order of 20%. This feature would be essential when searching for some energy dependence of polarization amount or angle (and, as stated in Section 1, this could constitute a clear signature of the presence of a black hole). We also note that, since the charge collected by the GEM is not subdivided, it could be exploited to get a higher signal to noise ratio and, finally, a better energy resolution (possibly coupled to an electronic chain with longer shaping time).

Being a pixel device, the instrument has intrinsic good imaging capabilities. The barycentre of the charge cluster is the rawest guess of photon conversion point, but we have already developed more sophisticated algorithms, based on charge release asymmetry, to do the job. To test them we let radiation enter the detector through collimators perforated with some patterns. In figure 8 the results are shown for a collimator with $500\mu m$ diameter holes, with $1mm$ pitch. MPGD imaging capabilities, by themselves very interesting, could also be used to improve the rejection of background due to walls.

3.3. MPGD polarimetric sensitivity and future perspectives

Although the aim of our tests was the measurement of MPGD polarization sensitivity in terms of modulation factor, collected data and performed simulations[10] allow to reliably evaluate the Minimum Detectable Polarization of our instrument, if placed at the focus of a X-ray optics. In figure 9 the effective area of the MPGD, placed at the focus of the XEUS[11] optics, is shown in two different configurations, respectively optimized for the *low-energy* band (0.1 - 2 keV) and the *high energy* one (2 - 10 keV). We want to note here that the reached polarimetric sensitivity of the MPGD, even if evaluated following a very conservative approach, already allows to perform a significant number of the measurements foreseen in the literature. In table 1 we report the MDP, in a representative sample of celestial objects, calculated for a detector basically identical to the tested prototype (with a greater collecting surface, to match the PSF of the optics and with a 50 μm Be window) if placed at the focus of the XEUS-1 X-ray optics. With typical integration time of the order of one day we could perform polarimetry of many AGNs at the level of 1% in the 2 - 10 keV energy band and energy-resolved polarimetry (in 3 or 4 bands) at the level of few percent; of course the situation would be even better for galactic sources. It's also interesting to note that the use of two MPGD, otpimized in different energy ranges, would allow to perform measurements covering the whole 0.6 - 10 keV energy band; the significant reduction of the necessary integration time would, in that case, compensate the increased complexity of the instrument.

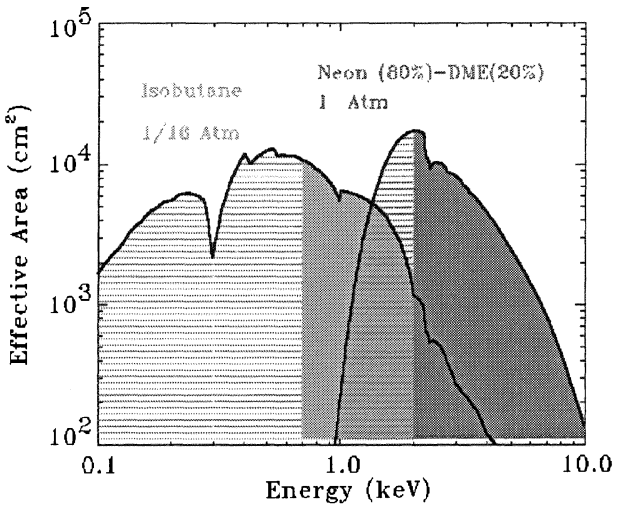

Figure 9. Effective area of two MPGD, optimized for low-energy and high-energy regions, placed at the focus of XEUS-1 X-ray optics. The bands of polarimetric sensitivity are represented in full colours.

Source	MDP (%)
CENA	0.6
NGC4151	0.7
NGC5548	0.8
MGC 6-30-15	1.2
Circinus Galaxy	2.8
IC4329A	0.7
Fairall 9	1.6
MKN501 (Outburst)	0.5
MKN421	0.7
3C273	0.9

Table 1. MDP in 10^5 sec (in the 2 - 10 keV energy band) evaluated for the MPGD, at the focus of the XEUS-1 optics, in some cases of physical interest.

4. CONCLUSIONS

Results quoted in this paper clearly show the potential of our approach; the tested prototype is much better of what has been done in the framework of standard techniques of X-ray polarimetry. MPGD can perform imaging and energy-resolved polarimetry (that Thomson and Bragg polarimeters cannot); moreover it provide imaging and spectral capabilities and fast timing down to 100 eV, even in the energy band in which the modulation factor can be seriously affected by the reduced track length. It is self triggering and, being truly 2D, it does not require rotation, with clear advantages for space applications. The new instrument could fully exploit the potential of a X-ray optics and, with great focal length, it could finally make X-ray polarimetry a *routine* observational technique.

ACKNOWLEDGMENTS

This research is partially funded by Agenzia Spaziale Italiana (ASI).

REFERENCES

1. P. Meszaros, R. Novick, G. A. Chanan, M. C. Weisskopf, A. Szentgyorgyi, *Astrophysical implications and observational prospects of X-ray polarimetry*, The Astrophysical Journal, vol. 324, pp. 1056-1067, 1988.
2. M. C. Weisskopf, G. G. Cohen, H. L. Kenstenbaum, K. S. Long, R. Novick, R. S. Wolff, *Measurement of the X-ray polarization of the Crab Nebula*, The Astrophysical Journal, vol. 208, pp. L125-L128, 1976.
3. J. Poutanen, *Relativistic jets in Blazars: polarization of radiation*, The Astrophysical Journal Supplement Series, vol. 92, pp. 607-609, 1994.
4. G. G. Pavlov, V. E. Zavlin, *Polarization of Thermal X-rays from Isolated Neutron Stars*, The Astrophysical Journal, vol. 529, pp. 1011-1018, 2000.
5. T. Kii, *X-ray Polarizations from Accreting Strongly Magnetized Neutron Stars: Case Studies for the X-ray Pulsars 4U 1626-67 and Hercules X-1*, Publ. Astron. Soc. Japan, vol. 39, pp. 781-800, 1987.
6. R. F. Stark, P. A. Connors, *Observable gravitational effects on polarized radiation coming from near a black hole*, Nature, vol. 269, pp. 128-129, 1977.
7. W. Heitler, *The Quantum Theory of Radiation*, Oxford University Press, 1970.
8. E. Costa, P. Soffitta, R. Bellazzini, A. Brez, N. Lumb, G. Spandre, *An efficient photoelectric X-ray polarimeter for the study of black holes and neutron stars*, Nature, vol. 411, pp. 662-664, 2001.
9. F. Sauli, *GEM: a new concept for electron amplification in gas detectors*, Nucl. Instr. Meth., volA. 386, pp. 531-534, 1997.
10. R. Bellazzini, F. Angelini, L. Baldini, A. Brez, E. Costa, G. di Persio, L. Latronico, M. M. Massai, N. Omodei, L. Pacciani, P. Soffitta , G. Spandre, *A novel gaseus X-ray polarimeter: data analysis and simulation*, Proceedings of Astronomical Telescopes and Instrumentation, Waikoloa, 22 - 28 August 2002.
11. M. Badvaz et al., *Status of the X-ray Evolving Universe Spectroscopy mission (XEUS)*, Proc. SPIE, vol 4138, pp. 69-78, 2000.